Calibration of groundwater seepage on the spatial distribution of the stream network to assess catchment-scale hydraulic conductivity

Ronan Abhervé[1], Alexandre Gauvain[1,4], Clément Roques[1,2], Laurent Longuevergne[1], Stéphane Louaisil[3],
Luc Aquilina[1], Jean-Raynald de Dreuzy[1]

[1]Univ Rennes, CNRS, Geosciences Rennes - UMR 6118, F-35000 Rennes, France
[2]Centre for Hydrology and Geothermics (CHYN), Université de Neuchâtel, Neuchâtel, Switzerland
[3]Eau du Bassin Rennais, Rennes, France
[4]Geosophy, Paris, France

Correspondence to: Ronan Abhervé (ronan.abherve@univ-rennes1.fr, ronan.abherve@gmail.com)

Abstract

To supplement the use of hydraulic tests and assess catchment-scale hydraulic conductivity (K), we propose a methodology for shallow aquifers only based on the Digital Elevation Model (DEM) and on the observation of the stream network. The methodology requires the groundwater system to be a main determinant of the stream density and extension. It assumes that the perennial stream network is set by the intersection of the groundwater table with the topography. The topographical structures and the subsurface hydraulic conductivity divided by the recharge rate K/R determine the groundwater table depth and the development of the stream network. Using a parsimonious 3D groundwater flow model, we calibrate K/R by minimizing newly defined distances between the simulated groundwater seepage zones and the observed stream network. Deployed on 24 selected headwater catchments from 12 to 141 km² located in north-western France, the method successfully matches the stream network in 80% of the cases and provides catchment-scale hydraulic conductivities between 9 x 10⁻⁶ and 9 x 10⁻⁵ m s⁻¹ for shallow aquifers sedimentary and crystalline rocks. Results show a high sensitivity of K to the density and extension of the low-order streams and limited impacts of the DEM resolution as long the DEM remains consistent with the stream network observations. With the emergence of global remote-sensing databases combining information of high-resolution DEM and stream network, this approach will contribute to assess hydraulic properties of in shallow headwater aquifers.

1   Introduction

Evaluating the availability of water resources and its evolution under global changes requires local knowledge on the storage
30   and transfer of water at the catchment scale (Fan et al., 2019). It involves the development of advanced hydrological models
resolving the important hillslope to catchment-scale processes (Refsgaard et al., 2010; Holman et al., 2012; Wada et al., 2010)
in a wide variety of high-stake areas (Elshall et al., 2020; Vergnes et al., 2020). Within the local hydrological cycle, aquifers
have a specific role ensuring the storage and transfer of water during and after recharge periods increasing the availability of
the resources (Fan, 2015; Fan et al., 2015) and sustaining surface systems in rain-free periods (Winter, 1999; Sophocleous,
35   2002; Alley et al., 2002; Anderson et al., 2015; Huscroft et al., 2018). Quantifying their contribution remains a challenge, as
their hydraulic properties have classically been constrained only by sparse borehole-scale characterization, hydraulic tests, and
head-based inverse problems (Anderson et al., 2015; Carrera et al., 2005). As global databases compiling hydraulic
conductivities give broad range of characteristic values by lithologies (Gleeson et al., 2014; Huscroft et al., 2018; Hartmann
and Moosdorf, 2012), it has been shown that they cannot be applied directly to local catchments (Reinecke et al., 2019; Tashie
40   et al., 2021; de Graaf et al., 2020). Analysis of stream discharge and borehole head dynamics have provided additional ways
to estimate effective hydraulic properties at larger scales (Brutsaert and Nieber, 1977; Vannier et al., 2014; Mendoza et al.,
2003; Troch et al., 2013) and to calibrate hydrological models (Eckhardt and Ulbrich, 2003; Etter et al., 2020; Chow et al.,
2016). However, this type of data faces the issue of deployment and maintenance of regional observation networks, engaging
the hydrological community to develop alternative methods to characterize ungauged catchments (Blöschl et al., 2019; Beven
45   et al., 2020).

We propose a method to quantify effective hydraulic conductivities of shallow aquifers from increasingly accessible
topographical and stream network observations when the density and extent of the stream system is dominantly controlled by
subsurface circulations. It is the case in temperate and wet climates for which surface and subsurface hydrological systems are
well connected (Cuthbert et al., 2019; Fan et al., 2013) and where the aquifer directly discharges into the stream network
50   (Haitjema and Mitchell-Bruker, 2005). Indeed, the discontinuous groundwater seepage network dominantly controls the
structure of the continuous stream network (Leibowitz et al., 2018; Pederson, 2001). At a given recharge rate, low permeable
aquifers display high groundwater table elevation and, consequently, dense stream networks in the upper part of the
catchments. At the opposite, highly permeable aquifers will display lower groundwater tables, higher discharge rates in fewer
seepage areas, and, consequently, sparser stream networks confined in the lower elevation valleys (Day, 1980; Lovill et al.,
55   2018; Dunne, 1975; Luo et al., 2016; Dietrich and Dunne, 1993; Godsey and Kirchner, 2014; Luijendijk, 2021; Prancevic and
Kirchner, 2019). Thus, the spatial extent of the stream network, its ramification (Vries, 1994; Devauchelle et al., 2012; Strahler,
1964) and the discharge rates in the seepage areas are controlled by the hydraulic conductivity K [L T^{-1}] divided by the recharge
rate R [L T^{-1}] (Haitjema and Mitchell-Bruker, 2005; Bresciani et al., 2016; Goderniaux et al., 2013; Gleeson and Manning,
2008).

According to Grayson and Blöschl (2000), observed spatial patterns are suitable for calibrating and evaluating distributed hydrologic models. Most approaches have provided means to predict the organization of the observed stream network but have not been designed to infer subsurface hydraulic properties. It is the case of studies that determine stream networks from the topographic information of the digital elevation model (DEM) when the modeled runoff accumulation exceeds a predefined threshold (Mardhel et al., 2021; Le Moine, 2008; Schneider et al., 2017; Luo and Stepinski, 2008; Lehner et al., 2013). Lumped parameter models, such as TOPMODEL (Beven and Kirkby, 1979), have also been extensively used to predict the spatial patterns of seepage areas at large scale (Merot et al., 2003; Blazkova et al., 2002; Güntner et al., 2004; Franks et al., 1998), but have not been used for the characterization of subsurface properties. Exceptions are the works proposed by Luo et al. (2010) and Stoll and Weiler (2010). Relying on explicit simulations of the spatial stream network, Stoll and Weiler (2010) have assessed the hydraulic properties in order to guide the calibration of hydrological models in ungauged basins. In their study, the authors optimize the parameters of their process-based hillslope model, primarily transmissivity, to get the best match between the simulated stream network and a reference. Luo et al. (2010) has calibrated a simplified 1D groundwater model on drainage dissection patterns to assess the spatial distribution of hydraulic conductivities. One of the main obstacles to the development of these approaches is gradually being resolved. Advances in remote sensing are progressively improving the description of global river networks (Yamazaki et al., 2019; Schneider et al., 2017; Lehner and Grill, 2013), wetlands (Tootchi et al., 2019) and soil moisture (Vergopolan et al., 2021). Lidar and high-resolution satellite imagery offers new opportunities to determine the surface characteristics of landscapes (Levizzani and Cattani, 2019; Blöschl et al., 2019) and, by extension, the hydrological parameters of local to continental ungauged catchments (Barclay et al., 2020; Dembélé et al., 2020).

We investigate the capacity to calibrate the catchment-scale effective hydraulic conductivities of shallow aquifers from the observed stream network with the help of a parsimonious 3D groundwater model to link groundwater flows and surface observations. We propose a novel performance criterion to assess the similarity between the simulated seepage areas and the observed stream network. We present the full methodology and its sensitivity to different stream network observation products on 24 catchments covering various geological contexts in north-western France. We discuss its relevance and perspectives to extensively characterize shallow aquifers from continuous surface information as proposed by Gleeson et al. (2021).

2   Materials and Methods

2.1   Model workflow

An overview of the model workflow is illustrated in Figure 1. Each block refers to a specific sub-section detailed below (from 2.2.1 to 2.2.5).

1. A digital elevation method (DEM) is used as the top boundary of the groundwater flow model (section 2.2.1);
2. 3D groundwater flow is solved in the model domain and simulated seepage areas are extracted (section 2.2.2);

3. A selected stream network independent of the DEM is taken as the observed reference (section 2.2.3);

4. The simulated seepage areas are compared with the observed stream network (section 2.2.4);

5. The dimensionless ratio K/R [-] is calibrated to find the best match between the simulated seepage areas and the extent of the observed stream network (section 2.2.5).
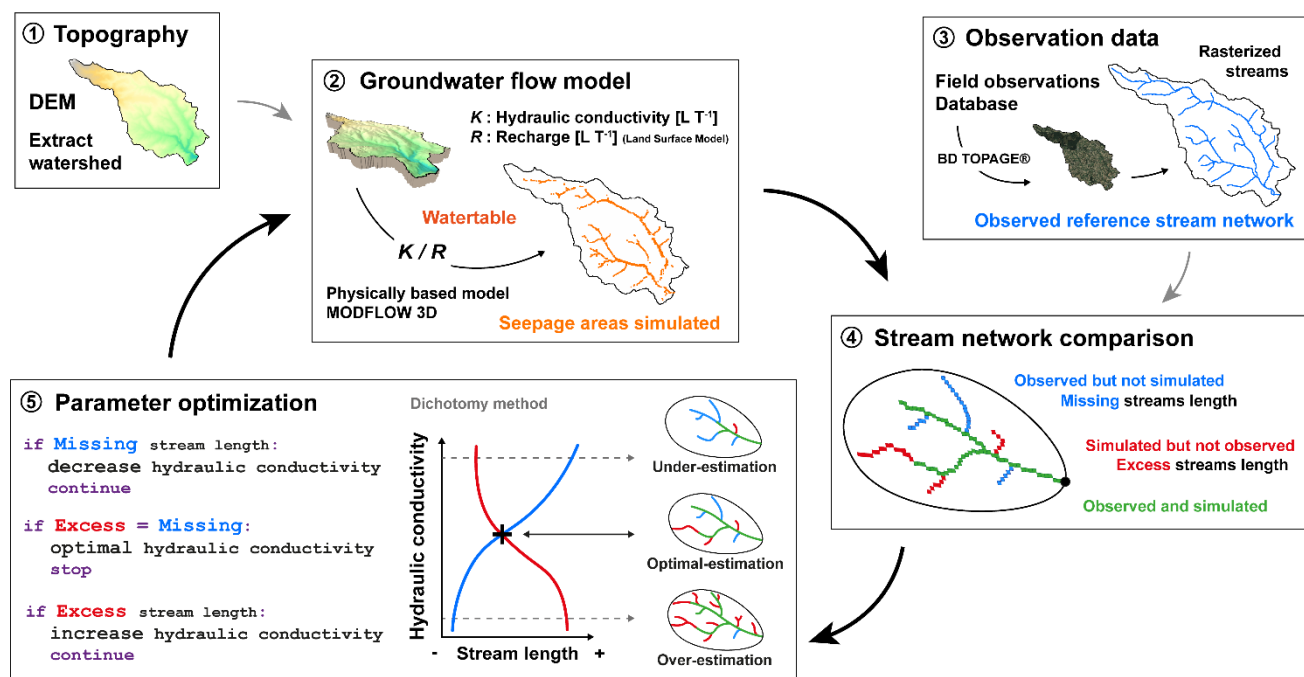
95

Figure 1. Workflow to constrain the hydraulic conductivity of the subsurface from an observed stream network.

2.1.1. Topography and model geometry

We first select the digital elevation model (DEM) that will be defined as the upper boundary of the groundwater model. In this

100 study, we use the 75 m grid resolution DEM available at the scale of France. It is generated from photogrammetric restitution and provided by BD ALTI (IGN, 2021). We also explore the impact of different DEM resolutions on the final estimations of K/R. We consider two higher resolution DEMs of 5 m and 25 m also provided by BD ALTI. For coarser resolutions, the 25 m DEM was downsampled with nearest neighbour option to larger cell sizes, i.e. 100 m, 200 m, and 300 m.

Geospatial processing is performed using the software WhiteBoxTools available in Python (Lindsay, 2016), labelled *WBT* in

105 the following. All functions of *WBT* used are quoted in brackets in the following. First, the raw DEM is corrected by filling all depressions and by removing flat areas (*WBT.FillDepressions*) to ensure continuous flow between grid cells. The vector point shapefile of the outlet is moved to the location coincident with the highest flow accumulation value

(*WBT.D8FlowAccumulation*) within a specified maximum distance taken as twice the DEM resolution (e.g. 150 m for a 75 m resolution DEM) (*WBT.SnapPourPoints*). A flow direction raster (*WBT.D8Pointer*) is used to extract the drainage basin 110 (*WBT.Watershed*).

2.1.2. Groundwater flow model

The MODFLOW software suite is used to solve the depth-integrated groundwater flow equation under steady state conditions (Eq. (1)) using a three-dimensional finite difference approach (Harbaugh, 2005; Niswonger et al., 2011):

$$\frac{\partial}{\partial x}\left[h\,K_{xx}\,\frac{\partial h}{\partial x}\right] + \frac{\partial}{\partial y}\left[h\,K_{yy}\,\frac{\partial h}{\partial y}\right] + \frac{\partial}{\partial x}\left[h\,K_{zz}\,\frac{\partial h}{\partial z}\right] = W \tag{1}$$

where h [L] is the hydraulic head, K [L T^{-1}] is the hydraulic conductivity along the x, y, and z coordinate axes, W [T^{-1}] is the 115 volumetric flux per unit volume from the porous medium.

We use the FloPy Python package (Bakker et al., 2016) to set and handle simulations. To reduce uncertainties linked to potential flow across topographic boundaries, a buffer zone is added to the topographical catchment boundaries, increasing the modelled domain area by 10 %. The model domain is discretized using the regular mesh of the DEM. In agreement with field observations in the region, the thickness of the domain is set to a constant value of 30 m representing the typical depth of the 120 interface between the weathered/fractured zone and the fresh bedrock (Kolbe et al., 2016; Dewandel et al., 2006; Roques et al., 2016). The hydraulic conductivity, K, is assumed to be uniform and isotropic. The recharge R is uniform over the domain with the top boundary set in the MODFLOW model as a drain to simulate head-dependent inflows (recharge) and outflows (discharge) (Harbaugh, 2005). Recharge operates on each cell while seepage areas and groundwater discharge only occur where the water table reaches the surface. The topography, the recharge and the aquifer thickness being fixed, the elevation of 125 the groundwater table is only controlled by the hydraulic conductivity. The porosity of the aquifer does not intervene at steady state.

2.1.3. Observation data of the stream network

The observed stream network is extracted from the most precise hydrographic network database available for France, the BD TOPAGE, as a vector format at scale of 1:10 000 (IGN and OFB, 2019). The main vector file labelled "Cours d'eau" (Rivers) 130 of the BD TOPAGE represents a majority of perennial sections of the stream network, i.e. filled and/or continuous-flow segments throughout the year. Note that the information classifying perennial or intermittent streams collected in the database is still under development to gain accuracy (Schneider et al., 2017). It has been rasterized at the grid resolution of the groundwater flow model to compare it to the simulated stream network (*WBT.VectorLinesToRaster*). Due to the uncertainty of the positioning of the stream network vector with respect to the DEM, the error is of the order of a pixel of the rasterization 135 (plus or minus 75 m). The influence of this error is analyzed in the results presented in section 3.1 (Figure 4). We also consider 5 other hydrographic network products to quantify their impact on the estimation of K/R. These products were compiled in

vector format from 3 different sources: the global-scale database HydroRIVERS (cases A), the French database BD TOPAGE (cases B, C and D), and local scale inventories (cases E and F) performed within the framework of the SAGE (Schéma d'Aménagement et de Gestion des Eaux, in French). Compared to the BD TOPAGE database, the HydroRivers product is

140 derived from a processing of DEM of lower resolution (approximately 500 m at the equator), while the local inventories are completed by more detailed field observations. More information on these products can be found in Appendix A.

2.1.4. Evaluation of the simulated seepage patterns and calibration criterion

For each pixel where seepage is simulated by the groundwater flow model, we trace the nearest downslope flowpath to the observed stream and compute its distance D_{so} [L] (*WBT.TraceDownslopeFlowpaths*) (Figure 2). The discontinuous pattern of

145 pixels with seepage is then converted into a continuous simulated stream network (Figure 2).
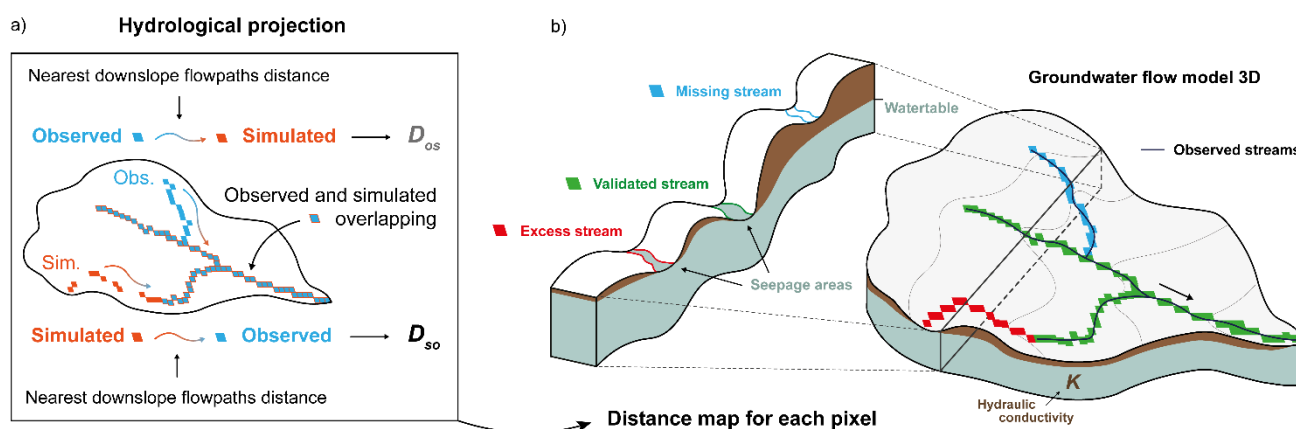
Figure 2. a) Definition of the main metrics used for calibration, with $\overline{D_{so}}$, the average distance of D_{so} from observed stream pixels (in blue) to the nearest (downslope flowpath) simulated seepage zone (in orange), and $\overline{D_{os}}$ the average distance of D_{os} between simulated seepage pixels to the nearest (downslope flowpath) observed stream. b) 3D conceptual diagram of the groundwater flow

150 **model and of a cross section through the catchment. Continuous streams are generated from pixels where the simulated water table intercepts the topography. By comparison with the observed stream network, some of the simulated streams are correctly estimated (valid in green), over-estimated (excess in red), or under-estimated (missing in blue).**

The distances of the simulated stream network to the observed one are averaged and labelled $\overline{D_{so}}$.

155 (*WBT.DownslopeDistanceToStream*). High $\overline{D_{so}}$ values are characteristic of stream networks extending far away from the observed steams. We also compute the mean distance of the observed to the simulated stream networks following a similar procedure. The distance D_{os} [L] from each observed stream network pixel to the simulated stream is computed along the steepest downslope path. In the following, we consider its average $\overline{D_{os}}$ obtained over all pixels of the observed streams. High $\overline{D_{os}}$ values are characteristic of underdeveloped stream network. The minimum absolute difference between $\overline{D_{so}}$ and $\overline{D_{os}}$

160 (Eq. (2)), labelled J, is used as the calibration criterion expressing the closest match of the observed and simulated streams or, in other words, the most relevant combination of missing and excess streams (Figure 2):

$$J = |\overline{D_{so}} - \overline{D_{os}}| \qquad (2)$$

2.1.5. Estimate of the hydraulic conductivity

The K/R ratio is calibrated by minimizing the objective function (Appendix B) defined by Eq. (2). Optimization is performed by a dichotomy approach (Burden and Faires, 1985). Convergence criterion is reached when K/R varies by less than 1 %. The

165 optimal catchment scale effective hydraulic conductivity K_{optim} is derived from the optimized K/R ratio by considering the average groundwater recharge rate R estimated by the land surface model SURFEX (version 8.1), for EXternalized SURFace (Le Moigne et al., 2020) (for more detailed information, the reader is referred to https://www.umr-cnrm.fr/surfex/). Supplied by meteorological variables, SURFEX computes the energy and water fluxes at the interfaces between soil, vegetation, and atmosphere (Noilhan and Mahfouf, 1996). The groundwater recharge of SURFEX is computed as the proportion of the water

170 mobilized down to the aquifer after infiltrating through the soil column (Vergnes et al., 2020). SURFEX was supplied by the SAFRAN meteorological reanalysis (Vidal et al., 2010; Quintana-Seguí et al., 2008), available over the French metropolitan area at an 8 x 8 km resolution. Here, we consider that R is equal to the long-term average recharge rates computed over almost sixty years (1960-2019).

2.2 Study sites

175 The approach is applied on 24 selected catchments located in Brittany and Normandy (France) (Figure 3), where an oceanic and temperate climate prevails. The average catchment area ranges from 12 to 141 km^2 with an average of 58 km^2 (Table 1), which corresponds to an average of 10 300 elements for the domain model discretization. These catchments were selected because of the diversity of their geological and geomorphological settings. Most of them are also subject to extensive research activities for their importance in providing freshwater to the nearby cities (sites 1, 2, 3, 4, 5, 6, 15, 16, 18, 19) or flooding

180 dynamics (Sites 20, 21, 22, 23, 24). Some of these sites are also studied in collaboration with local stakeholders on issues related to water quality and river restoration (Sites 8, 9, 10, 11, 12, 13 ,14, 17, 18 19) or within observatories and research infrastructure (Site 7: Long-Term Socio-Ecological Research (LTSER) "Zone Atelier Armorique (ZAAr)" and Sites 17, 18, 19: French network of Critical Zone Observatories (OZCAR) "Ploemeur-Guidel CZO"). None of these catchments present any reservoir or stream obstacle that would significantly alter the stream network. The study sites cover 5 major lithologies

185 including: Brioverian schist (sedimentary rock), Paleozoic sandstone and schist (sedimentary rock), plutonic rocks (mainly granite), micaschist (metamorphic sedimentary rock) and limestone (sedimentary rock). Sites have a homogeneous lithology (1:1 000 000 scale) throughout the catchment except for 5 sites (Sites 7, 8, 17, 18, 19) that present 2 lithologies.
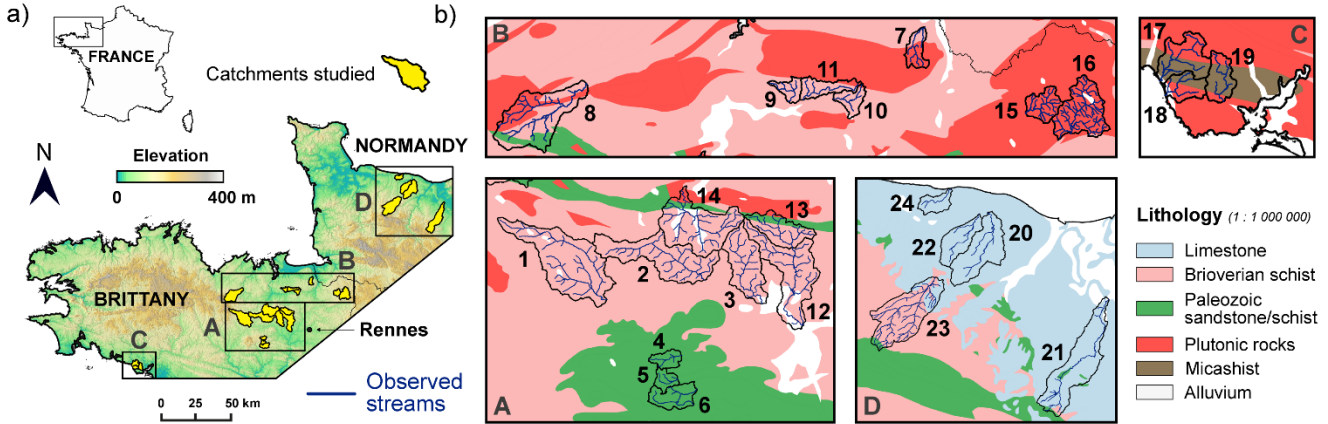
Figure 3. a) Localization of the studied catchments (Armorican Massif in Brittany and Normandy, North-Western part of France).
190 **b) Zoom on sites on top of a simplified geological map (1:1 000 000 scale) for the 4 center and right-hand side subpanels.**

3 Results

3.1 Application of the methodology

Before presenting the results obtained for all 24 study sites, we first illustrate the results of the methodology on one specific
195 site, the Gael catchment (Figure 3, Site 1). We provide details on the different steps of the numerical method and assess their
performance. Results are presented for 3 different values of K/R (Figure 4a). The dimensionless ratio K/R strongly controls
the spatial distribution of the hydraulic head, the shape of the groundwater table and its intersection with the surface (Figure
4a). An animated figure representing 2D map views of the simulated seepage areas as a function of K is available in the
supplementary material (Supplement 1). As K/R increases, the head gradient decreases, the aquifer progressively disconnects
200 from the surface and the seepage areas become sparser, mostly organized downstream, close to the catchment outlet. Inversely,
lower K/R values expand the seepage areas along the valleys and depressions towards the head of the catchment. Figure 4a
shows the sensitivity of the distances $\overline{D_{so}}$ and $\overline{D_{os}}$ varying between 0 m and 900 m. It confirms that the distance from the
observed to the simulated stream network $\overline{D_{so}}$ increases with K/R and inversely that the distance from the observed to the
simulated stream network $\overline{D_{os}}$ decreases with K/R. $\overline{D_{so}}$ and $\overline{D_{os}}$ intersect when the calibration criterion J is met, defining the
205 optimum value of the effective hydraulic conductivity through its ratio with the recharge K_{optim}/R. At this point, we define
the distance D_{optim} [m] as the average of $\overline{D_{so}}$ and $\overline{D_{os}}$ (Eq. (3)):

$$D_{optim} = \frac{\overline{D_{so}} + \overline{D_{os}}}{2}.$$ (3)

The smaller the value of D_{optim}, the better is the match of the simulated seepage pattern and the observed stream network. D_{optim} will thus be used as an indicator of the calibration performance. It will be compared to the DEM resolution DEM_{res} [m] as r_{optim} [-]:

$$r_{optim} = \frac{D_{optim}}{DEM_{res}}. \qquad (4)$$

210 r_{optim} should remain small to ensure the consistency of the observed and simulated stream networks. It will practically be limited to 2 considering that the mismatch cannot exceed the resolution of two pixels:

$$r_{optim} \leq 2. \qquad (5)$$

High-order streams are accurately predicted in all three simulations as shown by the green pixels (Figure 4a). However, low-order streams are obviously more sensitive and drive most of the variations of $\overline{D_{so}}$ and $\overline{D_{os}}$ as shown by the evolving red to green pixels when changing K/R. In other words, the calibration is controlled by the spatial extent of the streams from the

215 valleys to the headwaters following the topographic depressions. D_{optim} is equal to 143 m and remains smaller than twice the resolution of the DEM indicating a close match of the observed streams. Using the DEM resolution of 75 m as an indicator of uncertainty, K/R ranges between 3 054 and 10 000 (shaded area in Figure 4b, results of the maps are available in Appendix B), corresponding to an hydraulic conductivity ranging between 1.9 x 10^{-5} and 6.4 x 10^{-5} m s^{-1} for a recharge rate R of 201 mm y^{-1}. The optimal hydraulic conductivity K_{optim} estimated from the K_{optim}/R of 7 090 is equal to 4.5 x 10-5 m s^{-1}.
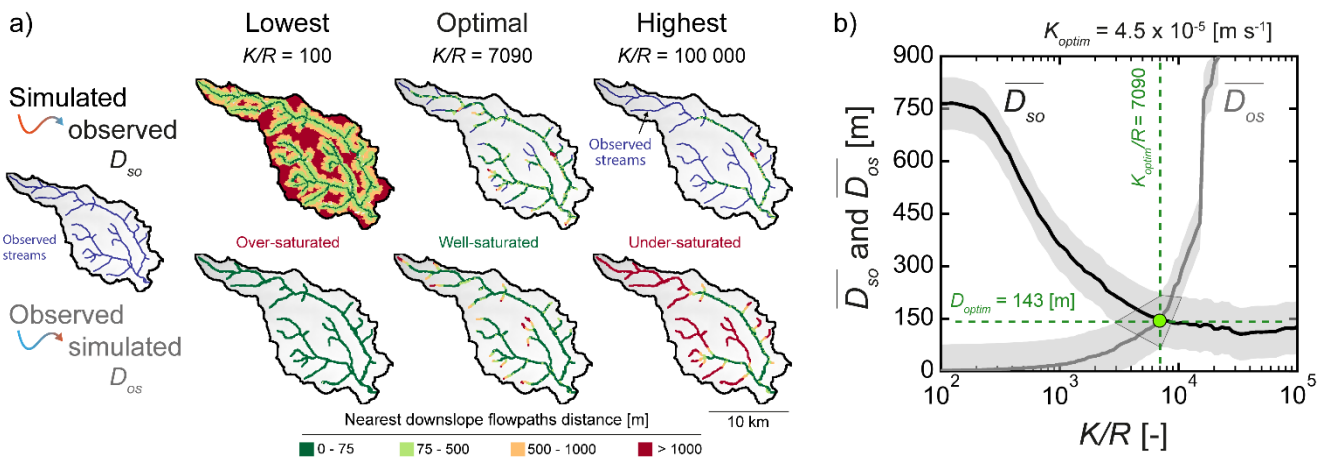
220

Figure 4. a) 2D map views of distances computed along the steepest slope from observed stream pixels to the nearest simulated ones (D_{os}) and from the seepage pixels to the nearest observed position of the stream network (D_{so}) for the Gael catchment. Results are presented for the lowest, optimal and highest K/R values explored. b) Average distances $\overline{D_{so}}$, and $\overline{D_{os}}$ as a function of the K/R. The shaded areas in grey around the curves correspond to the 75 m uncertainty range equal to the resolution the DEM. The optimal
225 **simulation is obtained for K_{optim}/R at the intersection between the two curves. At this point $\overline{D_{so}}$ and $\overline{D_{os}}$ are both equal to D_{optim} and in this case r_{optim} is close to 2. The hydraulic conductivity estimated K_{optim} is eventually derived by using the recharge rate provided by SURFEX.**

The method has been applied to the 23 other catchments displayed on Figure 3. Both $\overline{D_{so}}$ and $\overline{D_{os}}$ where found to systematically intersect defining an optimal effective hydraulic conductivity K_{optim} and a mean distance D_{optim}, both reported in Table 1.

230 Most D_{optim} distances remain limited to less than 2 pixels (Eq. (5)), showing the good consistency between the simulated stream network and the observed stream network (Figure 5). K_{optim}/R values range over one order of magnitude, from 1 239 to 14 883, resulting in K_{optim} values from 8.9 x 10^{-6} to 8.6 x 10^{-5} m s^{-1} (Figure 5). These values range from 2.4 x 10^{-6} to 2.5 x 10^{-4} m s^{-1} using the DEM resolution of 75 m as an uncertainty indicator. The model captures correctly the features of the observed stream network even in the presence of singular topographical features such as extended depressions or sharp changes

235 in slope (Gauvain et al., 2021; Schumm et al., 1995). This is especially the case on the site 7 where the seepage along the foot-slope issued by a steep slope transition (6 % on 1000 m of length) located along a lithological contact is well represented both by the model and in the observations as a significant and perennial groundwater spring/wetlands (Vautier et al., 2019; Kolbe et al., 2016).
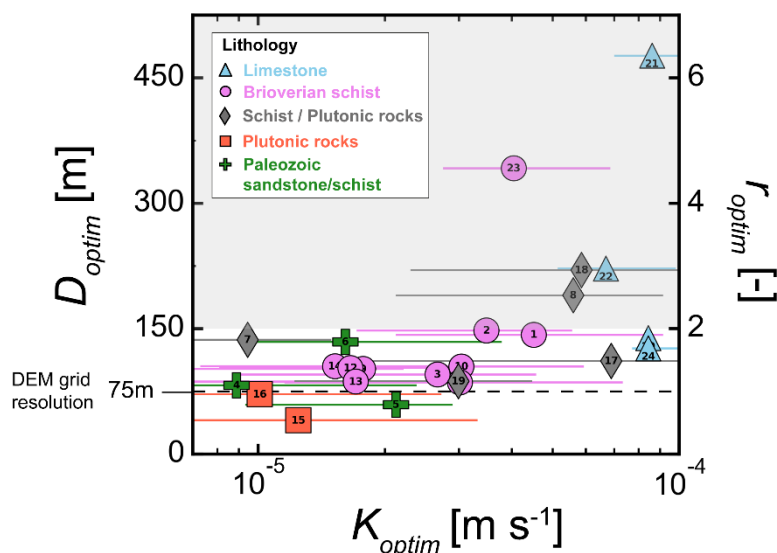
240 **Figure 5. D_{optim} and r_{optim} criteria as a function of K_{optim} estimated for the 24 sites. The shaded area corresponds to sites with a $r_{optim} > 2$. The DEM resolution is 75 m and the aquifer thickness is 30 m. The error bars correspond to the estimated K_{optim} considering the DEM resolution as an uncertainty indicator.**

245

Five sites (8, 18, 21, 22 and 23) display a lower match of the simulated and observed stream networks ($r_{optim} > 2$) with D_{optim} values ranging from 190 m to 477 m (Figure 5). The differences come essentially from the data themselves rather than from the model. Figure 6 maps the simulation results for these 5 sites. For the sites 21 and 22, the main errors come from a non-reported subsurface flow in the observed stream network within a karstic system however well represented by the model due

250   to a topographic depression along this area. For the site 23, the large error comes from inconsistencies between the observed stream network and the DEM. The depressions in the topography given by the DEM are far away from the observed stream network resulting in high distances and a high D_{optim} value. The site 18 displays similar issues where an extended seepage zone induced by a topographic depression is not reported on the observed river network. For site 8 only, differences come from the model and, more specifically, from the assumption of a uniform hydraulic conductivity. The predictions are more accurate

255   in the Brioverian schist and Paleozoic sandstone/schist areas than in the plutonic rocks where the drainage density is higher and for which the hydraulic conductivity should be lower.
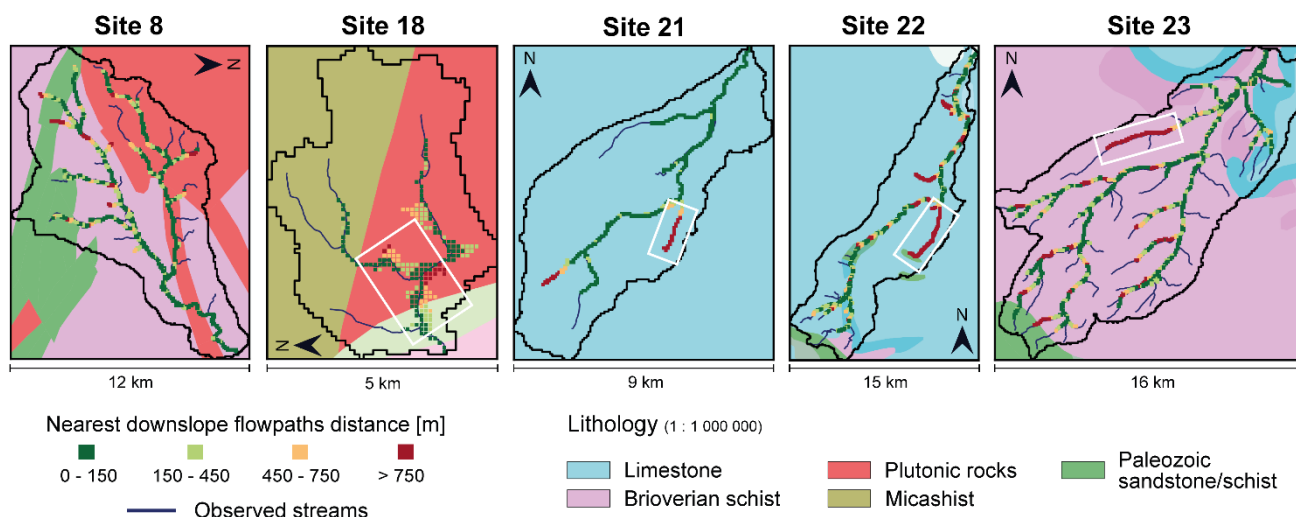
Figure 6. For the 5 sites corresponding to $r_{optim} > 2$, representation of the observed stream network on top of the simplified geological map (1:1 000 000 scale) with the downslope flowpaths distances of the simulated seepage areas projected to the observed
260   **streams. For site 8, differences are larger on the plutonic rocks. For the other sites, the white square identifies the area where errors are the largest.**

Table 1. Main landscape characteristics, model input parameters and estimated results of the 24 catchment sites studied.

Catchment	Site ID	Main lithology	Area [km^2]	Slope [%]	Drainage density [km^{-1}]	R [mm y^{-1}]	K_{optim}/R [-]	D_{optim} [m]	K_{optim} [m s^{-1}]	Mean of K_{optim} [m s^{-1}]
Basance	15	Plutonic rocks	26	4.0	1.8	237	1656	40	1.2×10^{-5}	1.1×10^{-5}
Nancon	16		65	3.3	1.5	237	1341	72	1.0×10^{-5}	
Serein	4	Paleozoic sandstone/schist	13	3.7	0.8	226	1239	82	8.9×10^{-6}	2.3×10^{-5}
Cheze	5		12	2.5	0.8	226	2960	59	2.1×10^{-5}	
Canut	6		28	2.2	0.7	215	2359	134	1.6×10^{-5}	
Gael	1	Brioverian schist	132	2.5	0.7	201	7090	143	4.5×10^{-5}	2.7×10^{-5}
Garun	2		96	2.4	0.7	175	6270	148	3.5×10^{-5}	
Vaunoise	3		62	2.7	0.8	168	5010	95	2.7×10^{-5}	
Estret	9		14	2.0	1.0	161	3487	102	1.8×10^{-5}	
Linonlac	10		16	2.9	0.8	164	5831	105	3.0×10^{-5}	
Bouteille	11		24	2.9	0.8	161	5919	86	3.0×10^{-5}	
Flume	12		134	2.9	0.9	161	3253	103	1.7×10^{-5}	
Vignoc	13		41	3.0	0.9	172	3136	87	1.7×10^{-5}	
Neal	14		95	2.7	0.9	175	2740	105	1.5×10^{-5}	
Seulles	23		134	4.7	1.1	274	4659	342	4.0×10^{-5}	
Home	7	Schist/ Plutonic rocks	19	2.4	1.0	190	1568	137	9.4×10^{-6}	4.5×10^{-5}
Arguenon	8		103	4.7	0.8	234	7559	190	5.6×10^{-5}	
Guidel	17		24	3.8	1.0	307	7090	111	6.9×10^{-5}	
Lannenec	18		13	3.1	0.9	234	7911	220	5.9×10^{-5}	
Ploemeur	19		15	2.9	0.9	307	3077	87	3.0×10^{-5}	
Mue	20	Limestone	99	1.5	0.4	179	14883	139	8.4×10^{-5}	8.0×10^{-5}
Laizon	21		141	2.2	0.5	182	14883	477	8.6×10^{-5}	
Thue	22		52	1.9	0.5	172	12305	222	6.7×10^{-5}	
Gronde	24		25	1.7	0.4	179	14883	127	8.4×10^{-5}	

265

3.2 Sensitivity of the calibrated hydraulic conductivity to input products, DEM resolution and model parameters

To further analyze the robustness of the method, we determine its sensitivity to the DEM resolution and to the observed stream network (Figure 7). The resolution of the DEM has only a minor influence on the optimal hydraulic conductivity when it remains consistent with the resolution of the stream network description. In the case of the Canut catchment (Figure 3, Site 6),

270 the simulated streams are consistent with the observed streams (Figure 7a1). The estimated K_{optim} values are close to each other from $1.2 \ 10^{-5}$ to $1.7 \ 10^{-5}$ m s^{-1}. The r_{optim} criterion (Eq. (4)) remains close to 1 (from 0.5 to 1.8), smaller than the threshold of 2 (Eq. (5)) (Figure 7a2). However, for the 5 m and 25 m resolutions tested, the distances $\overline{D_{so}}$ and $\overline{D_{os}}$ are highly sensitive to the mismatch between an increasingly accurate DEM and a coarsely defined stream network, the same issue as the one reported on several sites in the previous section. The main factor determining the distances is no longer the hydraulic

275 conductivity but the mismatch between the DEM and the observed stream network with r_{optim} values becoming larger (respectively 51.1 and 8.2 for the 5 m and 25 m resolutions tested). Because they highlight the inconsistency in the data between the DEM and the observed stream network, the finer DEM resolutions of 5 m and 25 m cannot be used, at least at this stage of the development of stream network observations and for this region. Resolutions of 75 m and coarser than 75 m lead however to consistent estimations of hydraulic conductivity showing the validity of the modeling approach.

280
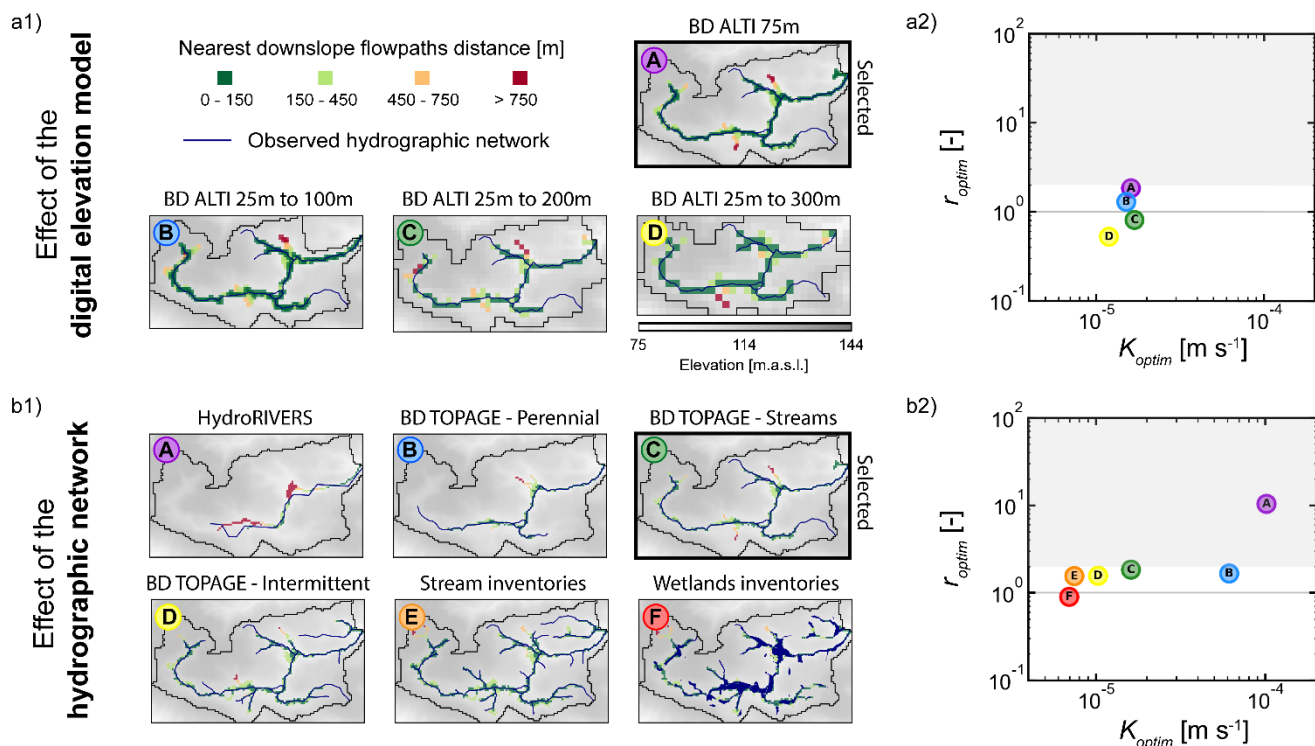
Figure 7. Sensitivity analysis of the method for the Canut catchment (Site 6) to a) the DEM resolution and b) the density and extent of the steam network displayed by different stream network products. Left pictures (a1, b1) show the downslope flowpaths distances of the simulated seepage areas projected onto the reference hydrographic network for K_{optim}. Right graphs (a2, b2) show the D_{ratio} as a function of K_{optim}.

As an additional indication of the quality of the method, the estimated hydraulic conductivity is sensitive to the extension of the observed stream network. We have systematically tested the method using six hydrographic networks issued by different global, national, and local databases (Figure 7b1). These products display largely evolving densities coming from the origin, nature, and scale of observations (Appendix A). For $DEM_{res} = 75$ m, the criterion r_{optim} (Eq. (4)) remains smaller than 2 for cases B to F qualifying them to estimate K_{optim} (Figure 7b2). For case A only, the global-scale product HydroRIVERS (Lehner et al., 2013) locates rivers away from the topographic valleys of the DEM issuing a D_{optim} value more than ten times larger than DEM_{res}. For cases B to F, the hydrographic network is well captured. Values of K_{optim} vary over one order of magnitude from 7 x 10^{-6} to 6 x 10^{-5} m s^{-1}. K_{optim} decreases with more extended and denser hydrographic networks. Indeed, dense river networks are generated by low hydraulic conductivities enabling high water table and headwater streams to develop upwards in the catchment (Figure 7b, E and F). Conversely, sparser hydrographic networks with streams located only at lower elevations require higher hydraulic conductivities (Figure 7b, A and B). The estimated hydraulic conductivity appears to be highly

sensitive to the elevation of wetlands and to the first-order stream locations confirming the capacity of the hydrographic density to inform the hydraulic conductivity.

4 Discussion and conclusion

We present a process-based groundwater modeling approach for the assessment of catchment-scale hydraulic conductivities that solely requires information on the density and spatial extent of the stream network. Based on this similar approach, Stoll and Weiler (2010) have estimated hydraulic conductivities in different catchments ranging from 10^{-6} to 10^{-7} m s^{-1} for metamorphic rocks, 10^{-5} m s^{-1} for sandstone, and 10^{-3} to 10^{-7} m s^{-1} for quaternary materials. Similar to our results, they show a strong control of transmissivity on the spatial distribution of simulated streams i.e., a larger spatial extent of the stream network when transmissivity is lower, and inversely. Luo et al. (2010) also proposed a similar modelling strategy considering local drainage density map to constrain a groundwater analytical model. These authors found a high variability of hydraulic conductivity for volcanic aquifers in the Oregon Cascades, ranging from 10^{-8} to 10^{-6} m s^{-1} for the older landscapes, and from 10^{-5} to 10^{-2} m s^{-1} for younger ones. While they fixed the flow-path length equal to the topographical downslope distance to the nearest stream (Luo and Stepinski, 2008), we propose a more general approach based on the mapping of the groundwater seepage from 2D vertically integrated flow simulations. This approach presents the advantage to remain valid in conditions for which the water table is not a strict replicate of the topography (Haitjema and Mitchell-Bruker, 2005), and the seepage structure is discontinuous and partly disconnected from the topography. The method calibrates the dimensionless parameter K/R by matching the modeled groundwater seepage zones to the observed stream network minimizing their respective distances. The nearest downslope flowpath distances ($\overline{D_{so}}$ and $\overline{D_{os}}$) improve the Euclidean distance of the cell-by-cell and cell-by-neighborhood analysis (Franks et al., 1998; Güntner et al., 2004) by constraining the observed-to-simulated and simulated-to-observed stream networks to the topographical structures. The high sensitivity of the computed K/R with both the density and spatial extent of the observed stream network highlights the requirements to use high-quality observed stream products and, when necessary, to improve them. River maps available on national to global databases are often incomplete compared to local databases compiled by stakeholders on direct field observations leading to an overestimation of the effective hydraulic conductivities. Moreover, the results showed that the resolution of DEM should not be much higher than the resolution of the hydrographic network to ensure the consistency of the observed stream network with the DEM.

For the 19 catchments for which the method is successfully applied, the method predicts a distribution of K values that remains surprisingly restricted within one order of magnitude despite the broad range of lithological units investigated (Figure 5). However, within this low variability of estimated K, we found clear distinction between lithologies. For example, we found lower values of K for plutonic rocks dominated catchments, suggesting high water table elevation with high drainage density, while limestones are significantly more permeable with lower drainage density. Although our results show evidences that effective hydraulic conductivities are related to variations in dominant lithologies, it is also clear that other reported factors

like erosion, bedrock weathering and fracturing may tend to homogenize the hydraulic properties under similar

330   erosion/weathering settings (Luo et al., 2016; Yoshida and Troch, 2016; Jefferson et al., 2010; Litwin et al., 2022).

Global syntheses compiling accurate predictions of hydraulic properties of the subsurface are critically needed to predict water resources availabilities (Fan et al., 2019) in ungauged catchments (Sivapalan et al., 2003; Hrachowitz et al., 2013) and to assess the impact of hillslope- and catchment-scale hydrology on global change predictions (Taylor et al., 2013). The methodology presented in this article is aimed to be deployed at multiple spatial scales taking advantages of global-scale databases compiling

335   topographic, hydrologic, and climatic information. Such deployment would leverage the current innovations in remote sensing and crowdsourcing (Etter et al., 2020) that now provide high resolution surface DEM products (Hawker et al., 2022; Yamazaki et al., 2017) and mapping of perennial stream networks (Fovet et al., 2021; Messager et al., 2021; Grill et al., 2019).

Appendices

Appendix A: Hydrographic network products information.

Global database: HydroRIVERS (available on this website: https://www.hydrosheds.org/page/hydrorivers) (Linke et al., 2019) is derived from HydroSHEDS (Lehner et al., 2013), a mapping product that provides hydrographic information for regional and global-scale applications, based on a grid resolution of 15 arc-seconds (approximately 500 m at the equator).

National database: The BD TOPAGE (available on this website: https://bdtopage.eaufrance.fr) database classifies streams as perennial or intermittent based on historical photogrammetric reconstructions.

Local database: The local stream and wetland inventory maps are based on observations and field surveys validated by the "Schéma d'Aménagement et de Gestion des Eaux (SAGE) (available on this website: https://sdage-sage.eau-loire-bretagne.fr/home.html).

Appendix B: Objective function of the calibration criteria.
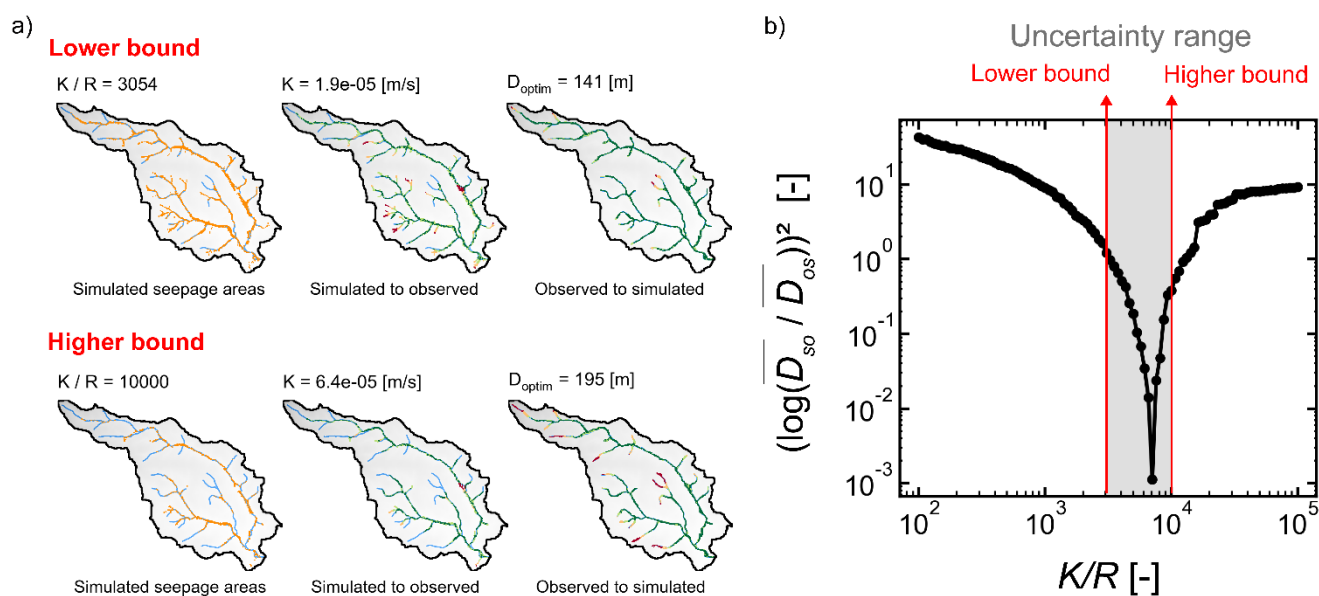
Fig. B1. a) 2D map views of simulated seepage areas and nearest downslope flowpaths distances (simulated to observed and observed to simulated) for the two K/R at the bounds of the uncertainty (lower and higher). b) Objective function based on the developed performance criteria obtained for the Gael (Site 1) catchment.

Supplements

Supplement 1: Evolution of the simulated hydrographic network as a function of *K*.

The animated figure in a *.gif format is provided in a *.zip archive.

360 **Fig. S1. Animated figure at the scale of the Gael catchment representing the 2D map views of simulated seepage areas and nearest downslope flowpaths distances (simulated to observed and observed to simulated). The maps come from an exploration of a wide range *K/R* [100 to 100 000].**

Code and data availability

The code to test the method from an example is available online at the reviewers' request:

365 https://github.com/RonanAbherve/stream-network_beta

Author contribution

All co-authors were involved in conceptualization and identified the research questions. RA and AG developed the model, performed the simulations, and analyzed the results. All co-authors participated in the interpretation of the results. RA created the figures. RA prepared the first draft of the manuscript. All co-authors reviewed and edited the manuscript.

370 ## Competing interests

The authors declare that they have no conflict of interest.

Acknowledgments

This work was supported by "Eaux et Territoires" research chaire driven by the Fondation Rennes 1. Clément Roques acknowledges financial supports from the Rennes Métropole research chair "Ressource en Eau du Futur" and the European
375 project WATERLINE, project id CHIST-ERA-19-CES-006. Alexandre Guavain acknowledges funding from the RIVAGES Normands 2100 project. The investigations benefited from the support of OZCAR, H+.

References

380   Alley, W. M., Healy, R. W., LaBaugh, J. W., and Reilly, T. E.: Flow and storage in groundwater systems, Science (80-.)., 296, 1985–1990, https://doi.org/10.1126/science.1067123, 2002.

Anderson, M. P., Woessner, W. W., and Hunt, R. J.: Applied groundwater modeling : simulation of flow and advective transport, Second Edi., Elsevier, AP Academic press is an imprint of Elsevier, Amsterdam, ixi, 564 pp., 2015.

Bakker, M., Post, V., Langevin, C. D., Hughes, J. D., White, J. T., Starn, J. J., and Fienen, M. N.: Scripting MODFLOW Model
385   Development Using Python and FloPy, 54, 733–739, https://doi.org/10.1111/gwat.12413, 2016.

Barclay, J. R., Starn, J. J., Briggs, M. A., and Helton, A. M.: Improved Prediction of Management-Relevant Groundwater Discharge Characteristics Throughout River Networks, Water Resour. Res., 56, 1–19, https://doi.org/10.1029/2020WR028027, 2020.

Beven, K., Asadullah, A., Bates, P., Blyth, E., Chappell, N., Child, S., Cloke, H., Dadson, S., Everard, N., Fowler, H. J., Freer,
390   J., Hannah, D. M., Heppell, K., Holden, J., Lamb, R., Lewis, H., Morgan, G., Parry, L., and Wagener, T.: Developing observational methods to drive future hydrological science: Can we make a start as a community?, Hydrol. Process., 34, 868–873, https://doi.org/10.1002/hyp.13622, 2020.

Beven, K. J. and Kirkby, M. J.: A physically based, variable contributing area model of basin hydrology, Hydrol. Sci. Bull., 24, 43–69, https://doi.org/10.1080/02626667909491834, 1979.

395   Blazkova, S., Beven, K. J., and Kulasova, A.: On constraining TOPMODEL hydrograph simulations using partial saturated area information, Hydrol. Process., 16, 441–458, https://doi.org/10.1002/hyp.331, 2002.

Blöschl, G., Bierkens, M. F. P., Chambel, A., Cudennec, C., Destouni, G., Fiori, A., Kirchner, J. W., McDonnell, J. J., Savenije, H. H. G., Sivapalan, M., Stumpp, C., Toth, E., Volpi, E., Carr, G., Lupton, C., Salinas, J., Széles, B., Viglione, A., Aksoy, H., Allen, S. T., Amin, A., Andréassian, V., Arheimer, B., Aryal, S. K., Baker, V., Bardsley, E., Barendrecht, M. H., Bartosova,
400   A., Batelaan, O., Berghuijs, W. R., Beven, K., Blume, T., Bogaard, T., Borges de Amorim, P., Böttcher, M. E., Boulet, G., Breinl, K., Brilly, M., Brocca, L., Buytaert, W., Castellarin, A., Castelletti, A., Chen, X., Chen, Y., Chen, Y., Chifflard, P., Claps, P., Clark, M. P., Collins, A. L., Croke, B., Dathe, A., David, P. C., de Barros, F. P. J., de Rooij, G., Di Baldassarre, G., Driscoll, J. M., Duethmann, D., Dwivedi, R., Eris, E., Farmer, W. H., Feiccabrino, J., Ferguson, G., Ferrari, E., Ferraris, S., Fersch, B., Finger, D., Foglia, L., Fowler, K., Gartsman, B., Gascoin, S., Gaume, E., Gelfan, A., Geris, J., Gharari, S., Gleeson,
405   T., Glendell, M., Gonzalez Bevacqua, A., González-Dugo, M. P., Grimaldi, S., Gupta, A. B., Guse, B., Han, D., Hannah, D., Harpold, A., Haun, S., Heal, K., Helfricht, K., Herrnegger, M., Hipsey, M., Hlaváčiková, H., Hohmann, C., Holko, L., Hopkinson, C., Hrachowitz, M., Illangasekare, T. H., Inam, A., Innocente, C., Istanbulluoglu, E., Jarihani, B., et al.: Twenty-three unsolved problems in hydrology (UPH) – a community perspective, Hydrol. Sci. J., 64, 1141–1158, https://doi.org/10.1080/02626667.2019.1620507, 2019.

410 Bresciani, E., Goderniaux, P., and Batelaan, O.: Hydrogeological controls of water table-land surface interactions, Geophys. Res. Lett., 43, 9653–9661, https://doi.org/10.1002/2016GL070618, 2016.

Brutsaert, W. and Nieber, J. L.: Regionalized Drought Flow Hydrographs From a Mature Glaciated Plateau, Water Resour. Res., 13, 1977.

Burden, R. L. and Faires, J. D.: "2.1 The Bisection Algorithm", Numerical Analysis (3rd ed.), PWS Publishers, 1985.

415 Carrera, J., Alcolea, A., Medina, A., Hidalgo, J., and Slooten, L. J.: Inverse problem in hydrogeology, Hydrogeol. J., 13, 206–222, https://doi.org/10.1007/s10040-004-0404-7, 2005.

Chow, R., Frind, M. E., Frind, E. O., Jones, J. P., Sousa, M. R., Rudolph, D. L., Molson, J. W., and Nowak, W.: Delineating baseflow contribution areas for streams – A model and methods comparison, J. Contam. Hydrol., 195, 11–22, https://doi.org/10.1016/j.jconhyd.2016.11.001, 2016.

420 Cuthbert, M. O., Gleeson, T., Moosdorf, N., Befus, K. M., Schneider, A., Hartmann, J., and Lehner, B.: Global patterns and dynamics of climate–groundwater interactions, Nat. Clim. Chang., 9, 137–141, https://doi.org/10.1038/s41558-018-0386-4, 2019.

Day, D. G.: Lithologic controls of drainage density : a stud of six small rural catchments in New England , N . S . W ., 7, 339–351, 1980.

425 de Graaf, I., Condon, L., and Maxwell, R.: Hyper-Resolution Continental-Scale 3-D Aquifer Parameterization for Groundwater Modeling, Water Resour. Res., 56, 1–14, https://doi.org/10.1029/2019WR026004, 2020.

Dembélé, M., Hrachowitz, M., Savenije, H. H. G., Mariéthoz, G., and Schaefli, B.: Improving the Predictive Skill of a Distributed Hydrological Model by Calibration on Spatial Patterns With Multiple Satellite Data Sets, Water Resour. Res., 56, 1–26, https://doi.org/10.1029/2019WR026085, 2020.

430 Devauchelle, O., Petroff, A. P., Seybold, H. F., and Rothman, D. H.: Ramification of stream networks, Proc. Natl. Acad. Sci. U. S. A., 109, 20832–20836, https://doi.org/10.1073/pnas.1215218109, 2012.

Dewandel, B., Lachassagne, P., Wyns, R., Maréchal, J. C., and Krishnamurthy, N. S.: A generalized 3-D geological and hydrogeological conceptual model of granite aquifers controlled by single or multiphase weathering, J. Hydrol., 330, 260–284, https://doi.org/10.1016/j.jhydrol.2006.03.026, 2006.

435 Dietrich, W. E. and Dunne, T.: The channel head, Channel Netw. Hydrol., eds Beven, 175–219, 1993.

Dunne, T.: Formation and controls of channel networks, 1975.

Eckhardt, K. and Ulbrich, U.: Potential impacts of climate change on groundwater recharge and streamflow in a central European low mountain range, J. Hydrol., 284, 244–252, https://doi.org/10.1016/j.jhydrol.2003.08.005, 2003.

Elshall, A. S., Arik, A. D., El-Kadi, A. I., Pierce, S., Ye, M., Burnett, K. M., Wada, C. A., Bremer, L. L., and Chun, G.:
440   Groundwater sustainability: a review of the interactions between science and policy, Environ. Res. Lett., 15,
https://doi.org/10.1088/1748-9326/ab8e8c, 2020.

Etter, S., Strobl, B., Seibert, J., and van Meerveld, H. J. I.: Value of Crowd-Based Water Level Class Observations for
Hydrological Model Calibration, Water Resour. Res., 56, 1–17, https://doi.org/10.1029/2019WR026108, 2020.

Fan, Y.: Groundwater in the Earth's critical zone: Relevance to large-scale patterns and processes, Water Resour. Res., 51,
445   3052–3069, https://doi.org/10.1002/2015WR017037, 2015.

Fan, Y., Li, H., and Miguez-Macho, G.: Global Patterns of Groundwater Table Depth, Science (80-.)., 339, 940–943,
https://doi.org/10.1126/science.1229881, 2013.

Fan, Y., Richard, S., Bristol, R. S., Peters, S. E., Ingebritsen, S. E., Moosdorf, N., Packman, A., Gleeson, T., Zaslavsky, I.,
Peckham, S., Murdoch, L., Fienen, M., Cardiff, M., Tarboton, D., Jones, N., Hooper, R., Arrigo, J., Gochis, D., Olson, J., and
450   Wolock, D.: DigitalCrust - a 4D data system of material properties for transforming research on crustal fluid flow, 15, 372–
379, https://doi.org/10.1111/gfl.12114, 2015.

Fan, Y., Clark, M., Lawrence, D. M., Swenson, S., Band, L. E., Brantley, S. L., Brooks, P. D., Dietrich, W. E., Flores, A.,
Grant, G., Kirchner, J. W., Mackay, D. S., McDonnell, J. J., Milly, P. C. D., Sullivan, P. L., Tague, C., Ajami, H., Chaney, N.,
Hartmann, A., Hazenberg, P., McNamara, J., Pelletier, J., Perket, J., Rouholahnejad-Freund, E., Wagener, T., Zeng, X.,
455   Beighley, E., Buzan, J., Huang, M., Livneh, B., Mohanty, B. P., Nijssen, B., Safeeq, M., Shen, C., van Verseveld, W., Volk,
J., and Yamazaki, D.: Hillslope Hydrology in Global Change Research and Earth System Modeling, Water Resour. Res., 1737–
1772, https://doi.org/10.1029/2018WR023903, 2019.

Fovet, O., Belemtougri, A., Boithias, L., Marylise, J. C., Kevin, C., and Braud, I.: Intermittent rivers and ephemeral streams :
Perspectives for critical zone science and research on socio-ecosystems, 1–33, https://doi.org/10.1002/wat2.1523, 2021.

460   Franks, S. W., Gineste, P., Beven, K. J., and Merot, P.: On constraining the predictions of a distributed model: The
incorporation of fuzzy estimates of saturated areas into the calibration process, Water Resour. Res., 34, 787–797,
https://doi.org/10.1029/97WR03041, 1998.

Gauvain, A., Leray, S., Marçais, J., and Roques, C.: Geomorphological Controls on Groundwater Transit Times : A Synthetic
Analysis at the Hillslope Scale Water Resources Research, i, 1–22, https://doi.org/10.1029/2020WR029463, 2021.

465   Gleeson, T. and Manning, A. H.: Regional groundwater flow in mountainous terrain: Three-dimensional simulations of
topographic and hydrogeologic controls, Water Resour. Res., 44, https://doi.org/10.1029/2008WR006848, 2008.

Gleeson, T., Moosdorf, N., Hartmann, J., and van Beek, L. P. H.: A glimpse beneath earth's surface: GLobal HYdrogeology
MaPS (GLHYMPS) of permeability and porosity, Geophys. Res. Lett., 41, 3891–3898, https://doi.org/10.1002/

2014GL059856, 2014.

470 Gleeson, T., Wagener, T., Döll, P., Zipper, S., West, C., Wada, Y., Taylor, R., Scanlon, B., Rosolem, R., Rahman, S., Oshinlaja, N., Maxwell, R., Lo, M.-H., Kim, H., Hill, M., Hartmann, A., Fogg, G., Famiglietti, J., Ducharne, A., de Graaf, I., Cuthbert, M., Condon, L., Bresciani, E., and Bierkens, M.: GMD Perspective: the quest to improve the evaluation of groundwater representation in continental to global scale models, Geosci. Model Dev. Discuss., 1–59, https://doi.org/10.5194/gmd-2021-97, 2021.

475 Goderniaux, P., Davy, P., Bresciani, E., de Dreuzy, J. R., and Le Borgne, T.: Partitioning a regional groundwater flow system into shallow local and deep regional flow compartments, Water Resour. Res., 49, 2274–2286, https://doi.org/10.1002/wrcr.20186, 2013.

Godsey, S. E. and Kirchner, J. W.: Dynamic, discontinuous stream networks: Hydrologically driven variations in active drainage density, flowing channels and stream order, Hydrol. Process., 28, 5791–5803, https://doi.org/10.1002/hyp.10310,
480 2014.

Grayson, R. B. and Blöschl, G.: Spatial Patterns in Catchment Hydrology: Observations and Modelling, Cambridge, UK, 404 pp., 2000.

Grill, G., Lehner, B., Thieme, M., Geenen, B., Tickner, D., Antonelli, F., Babu, S., Borrelli, P., Cheng, L., Crochetiere, H., Ehalt Macedo, H., Filgueiras, R., Goichot, M., Higgins, J., Hogan, Z., Lip, B., McClain, M. E., Meng, J., Mulligan, M., Nilsson,
485 C., Olden, J. D., Opperman, J. J., Petry, P., Reidy Liermann, C., Sáenz, L., Salinas-Rodríguez, S., Schelle, P., Schmitt, R. J. P., Snider, J., Tan, F., Tockner, K., Valdujo, P. H., van Soesbergen, A., and Zarfl, C.: Mapping the world's free-flowing rivers, Nature, 569, 215–221, https://doi.org/10.1038/s41586-019-1111-9, 2019.

Güntner, A., Seibert, J., and Uhlenbrook, S.: Modeling spatial patterns of saturated areas: An evaluation of different terrain indices, Water Resour. Res., 40, 1–19, https://doi.org/10.1029/2003WR002864, 2004.

490 Haitjema, H. M. and Mitchell-Bruker, S.: Are water tables a subdued replica of the topography?, Ground Water, 43, 781–786, https://doi.org/10.1111/j.1745-6584.2005.00090.x, 2005.

Harbaugh, A. W.: MODFLOW-2005 : the U.S. Geological Survey modular ground-water model--the ground-water flow process, Techniques and Methods, https://doi.org/10.3133/tm6A16, 2005.

Hartmann, J. and Moosdorf, N.: The new global lithological map database GLiM: A representation of rock properties at the
495 Earth surface, Geochemistry, Geophys. Geosystems, 13, 1–37, https://doi.org/10.1029/2012GC004370, 2012.

Hawker, L., Uhe, P., Paulo, L., Sosa, J., Savage, J., Sampson, C., and Neal, J.: A 30 m global map of elevation with forests and buildings removed, Environ. Res. Lett., 17, 024016, https://doi.org/10.1088/1748-9326/ac4d4f, 2022.

Holman, I. P., Allen, D. M., Cuthbert, M. O., and Goderniaux, P.: Towards best practice for assessing the impacts of climate

change on groundwater, Hydrogeol. J., 20, 1–4, https://doi.org/10.1007/s10040-011-0805-3, 2012.

500 Hrachowitz, M., Savenije, H. H. G., Blöschl, G., McDonnell, J. J., Sivapalan, M., Pomeroy, J. W., Arheimer, B., Blume, T., Clark, M. P., Ehret, U., Fenicia, F., Freer, J. E., Gelfan, A., Gupta, H. V., Hughes, D. A., Hut, R. W., Montanari, A., Pande, S., Tetzlaff, D., Troch, P. A., Uhlenbrook, S., Wagener, T., Winsemius, H. C., Woods, R. A., Zehe, E., and Cudennec, C.: A decade of Predictions in Ungauged Basins (PUB)-a review, Hydrol. Sci. J., 58, 1198–1255, https://doi.org/10.1080/02626667.2013.803183, 2013.

505 Huscroft, J., Gleeson, T., Hartmann, J., and Börker, J.: Compiling and Mapping Global Permeability of the Unconsolidated and Consolidated Earth: GLobal HYdrogeology MaPS 2.0 (GLHYMPS 2.0), Geophys. Res. Lett., 45, 1897–1904, https://doi.org/10.1002/2017GL075860, 2018.

IGN: Le modèle numérique de terrain (MNT) maillé qui décrit le relief du territoire français à moyenne échelle BD ALTI® version 2021, Information Géographique sur l'Eau et Institut National de l'Information Géographique et Forestière, 2021.

510 IGN and OFB: Jeu de données des cours d'eau de France métropolitaine BD TOPAGE® version 2019, Office Français de la Biodiversité (OFB) - Information Géographique sur l'Eau et Institut National de l'Information Géographique et Forestière, 2019.

Jefferson, A., Grant, G. E., Lewis, S. L., and Lancaster, S. T.: Coevolution of hydrology and topography on a basalt landscape in the Oregon Cascade Range, USA, Earth Surf. Process. Landforms, 35, 803–816, https://doi.org/10.1002/esp.1976, 2010.

515 Kolbe, T., Marçais, J., Thomas, Z., Abbott, B. W., de Dreuzy, J.-R., Rousseau-Gueutin, P., Aquilina, L., Labasque, T., and Pinay, G.: Coupling 3D groundwater modeling with CFC-based age dating to classify local groundwater circulation in an unconfined crystalline aquifer, J. Hydrol., 543, 31–46, https://doi.org/10.1016/j.jhydrol.2016.05.020, 2016.

Lehner, B. and Grill, G.: Global river hydrography and network routing: Baseline data and new approaches to study the world's large river systems, Hydrol. Process., 27, 2171–2186, https://doi.org/10.1002/hyp.9740, 2013.

520 Lehner, B., Verdin, K., and Jarvis, A.: HydroSHEDS Technical Documentation Version 1.2, EOS Trans., 89, 26, 2013.

Leibowitz, S. G., Wigington, P. J., Schofield, K. A., Alexander, L. C., Vanderhoof, M. K., and Golden, H. E.: Connectivity of Streams and Wetlands to Downstream Waters: An Integrated Systems Framework, J. Am. Water Resour. Assoc., 54, 298–322, https://doi.org/10.1111/1752-1688.12631, 2018.

Levizzani, V. and Cattani, E.: Satellite Remote Sensing of Precipitation and the Terrestrial Water Cycle in a Changing Climate, 525 Remote Sens., 11, https://doi.org/10.3390/rs11192301, 2019.

Lindsay, J. B.: Whitebox GAT: A case study in geomorphometric analysis, Comput. Geosci., 95, 75–84, https://doi.org/10.1016/j.cageo.2016.07.003, 2016.

Linke, S., Lehner, B., Ouellet Dallaire, C., Ariwi, J., Grill, G., Anand, M., Beames, P., Burchard-Levine, V., Maxwell, S.,

Moidu, H., Tan, F., and Thieme, M.: Global hydro-environmental sub-basin and river reach characteristics at high spatial

530   resolution, Sci. Data, 6, 1–16, https://doi.org/10.1038/s41597-019-0300-6, 2019.

Litwin, D. G., Tucker, G. E., Barnhart, K. R., and Harman, C. J.: Groundwater Affects the Geomorphic and Hydrologic

Properties of Coevolved Landscapes, J. Geophys. Res. Earth Surf., 127, 1–36, https://doi.org/10.1029/2021JF006239, 2022.

Lovill, S. M., Hahm, W. J., and Dietrich, W. E.: Drainage from the critical zone: lithologic controls on the persistence and

spatial extent of wetted channels during the summer dry season, https://doi.org/10.1029/Water, 2018.

535   Luijendijk, E.: Transmissivity and groundwater flow exert a strong influence on drainage density, 1–32, 2021.

Luo, W. and Stepinski, T.: Identification of geologic contrasts from landscape dissection pattern: An application to the Cascade

Range, Oregon, USA, 99, 90–98, https://doi.org/10.1016/j.geomorph.2007.10.014, 2008.

Luo, W., Grudzinski, B. P., and Pederson, D.: Estimating hydraulic conductivity from drainage patterns-a case study in the

Oregon Cascades, Geology, 38, 335–338, https://doi.org/10.1130/G30816.1, 2010.

540   Luo, W., Jasiewicz, J., Stepinski, T., Wang, J., Xu, C., and Cang, X.: Spatial association between dissection density and

environmental factors over the entire conterminous United States, Geophys. Res. Lett., 43, 692–700,

https://doi.org/10.1002/2015GL066941, 2016.

Mardhel, V., Pinson, S., and Allier, D.: Description of an indirect method (IDPR) to determine spatial distribution of infiltration

and   runoff   and   its   hydrogeological   applications   to   the   French   territory,   J.   Hydrol.,   592,

545   https://doi.org/10.1016/j.jhydrol.2020.125609, 2021.

Mendoza, G. F., Steenhuis, T. S., Walter, M. T., and Parlange, J. Y.: Estimating basin-wide hydraulic parameters of a semi-

arid mountainous watershed by recession-flow analysis, J. Hydrol., 279, 57–69, https://doi.org/10.1016/S0022-

1694(03)00174-4, 2003.

Merot, P., Squividant, H., Aurousseau, P., Hefting, M., Burt, T., Maitre, V., Kruk, M., Butturini, A., Thenail, C., and Viaud,

550   V.: Testing a climato-topographic index for predicting wetlands distribution along an European climate gradient, Ecol. Modell.,

163, 51–71, https://doi.org/10.1016/S0304-3800(02)00387-3, 2003.

Messager, M. L., Lehner, B., Cockburn, C., Lamouroux, N., Pella, H., Snelder, T., Tockner, K., Trautmann, T., Watt, C., and

Datry, T.: Global prevalence of non-perennial rivers and streams, Nature, 594, 391–397, https://doi.org/10.1038/s41586-021-

03565-5, 2021.

555   Le Moigne, P., Besson, F., Martin, E., Boé, J., Decharme, B., Etchevers, P., Faroux, S., Habets, F., Lafaysse, M., Leroux, D.,

and Rousset-Regimbeau, F.: The Latest Improvements in SURFEX v8.0 of the Safran-Isba-Modcou Hydrometeorological

Model over France, Geosci. Model Dev. Discuss., 1–32, https://doi.org/10.5194/gmd-2020-31, 2020.

Le Moine, N.: Le bassin versant de surface vu par le souterrain : une voie d'amélioration des performances et du réalisme des

modèles pluie-débit ?, 348, 2008.

560   Niswonger, R. G., Panday, S., and Ibaraki, M.: MODFLOW-NWT , A Newton Formulation for MODFLOW-2005, U.S. Geol. Surv. Tech. Methods, 6, 0–44, 2011.

Noilhan, J. and Mahfouf, J. F.: The ISBA land surface parameterisation scheme, Glob. Planet. Change, 13, 145–159, https://doi.org/10.1016/0921-8181(95)00043-7, 1996.

Pederson, D. T.: Stream Piracy Revisited: A Groundwater-Sapping Solution, 2001.

565   Prancevic, J. P. and Kirchner, J. W.: Topographic Controls on the Extension and Retraction of Flowing Streams, Geophys. Res. Lett., 46, 2084–2092, https://doi.org/10.1029/2018GL081799, 2019.

Quintana-Seguí, P., Le Moigne, P., Durand, Y., Martin, E., Habets, F., Baillon, M., Canellas, C., Franchisteguy, L., and Morel, S.: Analysis of near-surface atmospheric variables: Validation of the SAFRAN analysis over France, J. Appl. Meteorol. Climatol., 47, 92–107, https://doi.org/10.1175/2007JAMC1636.1, 2008.

570   Refsgaard, J. C., Hojberg, A. L., Moller, I., Hansen, M., and Sondergaard, V.: Groundwater modeling in integrated water resources management--visions for 2020, Ground Water, 48, 633–648, https://doi.org/10.1111/j.1745-6584.2009.00634.x, 2010.

Reinecke, R., Foglia, L., Mehl, S., Herman, J. D., Wachholz, A., Trautmann, T., and Döll, P.: Spatially distributed sensitivity of simulated global groundwater heads and flows to hydraulic conductivity , groundwater recharge and surface water body 575   parameterization, 1–26, 2019.

Roques, C., Bour, O., Aquilina, L., and Dewandel, B.: High-yielding aquifers in crystalline basement: insights about the role of fault zones, exemplified by Armorican Massif, France, Hydrogeol. J., 24, 2157–2170, https://doi.org/10.1007/s10040-016-1451-6, 2016.

Schneider, A., Jost, A., Coulon, C., Silvestre, M., Théry, S., and Ducharne, A.: Global-scale river network extraction based on 580   high-resolution topography and constrained by lithology, climate, slope, and observed drainage density, Geophys. Res. Lett., 44, 2773–2781, https://doi.org/10.1002/2016GL071844, 2017.

Schumm, S. A., Boyd, K. F., Wolff, C. G., and Spitz, W. J.: A ground-water sapping landscape in the Florida Panhandle, 12, 281–297, 1995.

Sivapalan, M., Takeuchi, K., Franks, S. W., Gupta, V. K., Karambiri, H., Lakshmi, V., Liang, X., McDonnell, J. J., Mendiondo, 585   E. M., O'Connell, P. E., Oki, T., Pomeroy, J. W., Schertzer, D., Uhlenbrook, S., and Zehe, E.: IAHS Decade on Predictions in Ungauged Basins (PUB), 2003-2012: Shaping an exciting future for the hydrological sciences, Hydrol. Sci. J., 48, 857–880, https://doi.org/10.1623/hysj.48.6.857.51421, 2003.

Sophocleous, M.: Interactions between groundwater and surface water: the state of the science, Hydrogeol. J., 10, 52–67,

https://doi.org/10.1007/s10040-001-0170-8, 2002.

590 Stoll, S. and Weiler, M.: Explicit simulations of stream networks to guide hydrological modelling in ungauged basins, Hydrol. Earth Syst. Sci., 14, 1435–1448, https://doi.org/10.5194/hess-14-1435-2010, 2010.

Strahler, A. N.: Quantitative geomorphology of drainage basins and channel networks, Chow, V.T. Handb. Appl. Hydrol. McGraw-Hill, New York, 439–476, 1964.

Tashie, A., Pavelsky, T. M., Band, L., and Topp, S.: Watershed-Scale Effective Hydraulic Properties of the Continental United 595 States Journal of Advances in Modeling Earth Systems, 1–18, https://doi.org/10.1029/2020MS002440, 2021.

Taylor, R. G., Scanlon, B., Doll, P., Rodell, M., van Beek, R., Wada, Y., Longuevergne, L., Leblanc, M., Famiglietti, J. S., Edmunds, M., Konikow, L., Green, T. R., Chen, J. Y., Taniguchi, M., Bierkens, M. F. P., MacDonald, A., Fan, Y., Maxwell, R. M., Yechieli, Y., Gurdak, J. J., Allen, D. M., Shamsudduha, M., Hiscock, K., Yeh, P. J. F., Holman, I., and Treidel, H.: Ground water and climate change, Nat. Clim. Chang., 3, 322–329, https://doi.org/10.1038/nclimate1744, 2013.

600 Tootchi, A., Jost, A., and Ducharne, A.: Multi-source global wetland maps combining surface water imagery and groundwater constraints, Earth Syst. Sci. Data, 11, 189–220, https://doi.org/10.5194/essd-11-189-2019, 2019.

Troch, P. A., Berne, A., Bogaart, P., Harman, C., Hilberts, A. G. J., Lyon, S. W., Paniconi, C., Pauwels, V. R. N., Rupp, D. E., Selker, J. S., Teuling, A. J., Uijlenhoet, R., and Verhoest, N. E. C.: The importance of hydraulic groundwater theory in catchment hydrology: The legacy of Wilfried Brutsaert and Jean-Yves Parlange, Water Resour. Res., 49, 5099–5116, 605 https://doi.org/10.1002/wrcr.20407, 2013.

Vannier, O., Braud, I., and Anquetin, S.: Regional estimation of catchment-scale soil properties by means of streamflow recession analysis for use in distributed hydrological models, Hydrol. Process., 28, 6276–6291, https://doi.org/10.1002/hyp.10101, 2014.

Vautier, C., Abhervé, R., Labasque, T., Laverman, A. M., Guillou, A., Chatton, E., Dupont, P., Aquilina, L., and de Dreuzy, 610 J.-R.: Mapping gas exchanges in headwater streams with membrane inlet mass spectrometry, J. Hydrol., https://doi.org/10.1016/j.jhydrol.2019.124398, 2019.

Vergnes, J.-P., Roux, N., Habets, F., Ackerer, P., Amraoui, N., Besson, F., Caballero, Y., Courtois, Q., de Dreuzy, J.-R., Etchevers, P., Gallois, N., Leroux, D. J., Longuevergne, L., Le Moigne, P., Morel, T., Munier, S., Regimbeau, F., Thiéry, D., and Viennot, P.: The AquiFR hydrometeorological modelling platform as a tool for improving groundwater resource 615 monitoring over France: evaluation over a 60-year period, Hydrol. Earth Syst. Sci., 24, 633–654, https://doi.org/10.5194/hess-24-633-2020, 2020.

Vergopolan, N., Chaney, N. W., Pan, M., Sheffield, J., Beck, H. E., Ferguson, C. R., Torres-Rojas, L., Sadri, S., and Wood, E. F.: SMAP-HydroBlocks, a 30-m satellite-based soil moisture dataset for the conterminous US, Sci. Data, 8, 1–11,

https://doi.org/10.1038/s41597-021-01050-2, 2021.

620 Vidal, J. P., Martin, E., Franchistéguy, L., Baillon, M., and Soubeyroux, J. M.: A 50-year high-resolution atmospheric reanalysis over France with the Safran system, Int. J. Climatol., 30, 1627–1644, https://doi.org/10.1002/joc.2003, 2010.

Vries, J. J. De: Dynamics of the interface between streams and groundwater systems in lowland areas, with reference to stream net evolution, 1694, 1994.

Wada, Y., van Beek, L. P. H., van Kempen, C. M., Reckman, J., Vasak, S., and Bierkens, M. F. P.: Global depletion of 625 groundwater resources, Geophys. Res. Lett., 37, https://doi.org/10.1029/2010gl044571, 2010.

Winter, T. C.: Relation of streams, lakes, and wetlands to groundwater flow systems, Hydrogeol. J., 7, 28–45, https://doi.org/10.1007/s100400050178, 1999.

Yamazaki, D., Ikeshima, D., Tawatari, R., Yamaguchi, T., O'Loughlin, F., Neal, J. C., Sampson, C. C., Kanae, S., and Bates, P. D.: A high-accuracy map of global terrain elevations, Geophys. Res. Lett., 44, 5844–5853, 630 https://doi.org/10.1002/2017GL072874, 2017.

Yamazaki, D., Ikeshima, D., Sosa, J., Bates, P. D., Allen, G. H., and Pavelsky, T. M.: MERIT Hydro: A High-Resolution Global Hydrography Map Based on Latest Topography Dataset, Water Resour. Res., 55, 5053–5073, https://doi.org/10.1029/2019WR024873, 2019.

Yoshida, T. and Troch, P. A.: Coevolution of volcanic catchments in Japan, Hydrol. Earth Syst. Sci., 20, 1133–1150, 635 https://doi.org/10.5194/hess-20-1133-2016, 2016.